

# Constraints on the parameters of radiatively decaying dark matter from the dark matter halo of the Milky Way and Ursa Minor

A. Boyarsky,<sup>1,2,3</sup> J. Nevalainen,<sup>4</sup> and O. Ruchayskiy<sup>5</sup>

<sup>1</sup>*CERN, PH-TH, CH-1211 Geneve 23, Switzerland*

<sup>2</sup>*École Polytechnique Fédérale de Lausanne, Institute of Theoretical Physics,  
FSB/ITP/LPPC, BSP 720, CH-1015, Lausanne, Switzerland*

<sup>3</sup>On leave of absence from *Bogolyubov Institute of Theoretical Physics, Kyiv, Ukraine*

<sup>4</sup>*Helsinki University Observatory*

<sup>5</sup>*Institut des Hautes Études Scientifiques, Bures-sur-Yvette, F-91440, France*

(Dated: February 7, 2020)

Using the recent *XMM-Newton* PN blank sky data, we improve the earlier restrictions on parameters of the warm dark matter (DM) in the form of sterile neutrino (by as much as the order of magnitude at masses  $\sim 3.5$  keV). The results are obtained from non-observing DM decay line in the X-ray spectrum of the Milky Way. We also present similar constraint coming from the recent *XMM-Newton* observation of Ursa Minor – dark, X-ray quiet dwarf spheroidal. Although this observation has relatively poor statistics, the constraints are comparable to those, recently obtained using observations of Large Magellanic Cloud or M31. This confirms recent proposal that dwarf satellites of the MW are very interesting candidates for the DM search and should be studied dedicatedly on this purpose.

PACS numbers: 95.35.+d, 14.60.Pq, 95.85.Nv

## I. INTRODUCTION

Last year saw a lot of activity, devoted to searching of the decay signals of the DM particle in X-ray spectra of various astrophysical objects [1, 2, 3, 4, 5, 6]. It was noticed long ago [7] that a right-handed neutrino with masses in the keV range presents a viable *warm dark matter* (WDM) candidate. Such a particle possesses specific radiative decay channel and therefore one can search for its decay line in the X-ray spectra of astrophysical objects [8, 9].

Recently, the interest to the sterile neutrino as a DM candidate has been greatly revitalized. First, the discovery of neutrino oscillations (see e.g. [10] for a review) strongly suggest existence of right-handed neutrinos. Indeed, probably the easiest way to explain the data on oscillations is via adding several right handed, or *sterile* neutrinos, to the Standard Model. It has been demonstrated recently in Refs. [11, 12] that a simple extension of the Standard Model by three singlet fermions with masses smaller than the electroweak scale (dubbed the  $\nu$ MSM in [11]) allows to accommodate the data on neutrino masses and mixings, allows to explain baryon asymmetry of the Universe and provides a candidate for dark matter particle in the form of the lightest of the sterile neutrinos.

Secondly, *warm* DM with the mass of particle in keV range can ease the problem of the dark halo structures in comparison with the cold dark matter scenario [13, 14]. Additionally, by determining the matter power spectrum from Lyman- $\alpha$  forest data from SDSS, Refs. [15, 16] argued that the mass of the DM particles should be in the range  $\gtrsim 10$  keV ( $\gtrsim 14$  keV in the case of Ref. [15]). At the same time, studies of the Fornax dwarf spheroidal galaxy [14, 17] are in disagreement with the predictions

of CDM models and suggest lower than in [15, 16] mass for DM particle  $M_{\text{DM}} \sim 2$  keV. The latter result is in agreement with the earlier studies of [18, 19], which used different dataset. For other applications of the keV range sterile neutrinos see e.g. [20, 21, 22, 23, 24].

It was argued in [3, 4] that the preferred targets for observations are objects from the Local Halo, including our own Milky Way and its satellites. In particular, Ref. [3] showed that the best objects should be the dwarf spheroidals (Ursa Minor, Draco, etc). Indeed, these objects are X-ray quiet, while at the same time one expects from them the DM decay signal, comparable with that of from galaxy clusters. As at the time of writing of Ref. [3] no public data for aforementioned dwarf spheroidals were available, the observations of the core of Large Magellanic Cloud (LMC) were used to produce the strongest restrictions on parameters of the sterile neutrino. It was stressed in [3] that other dwarf satellite galaxies should be studied as well, in order to minimize uncertainties related to the DM modeling in every particular object. In this paper we continue studies of the dwarf satellites of the MW with the analysis of the data from *XMM-Newton* observation of Ursa Minor and confirm the restrictions of Ref. [3].

It was also shown in Ref. [3] that the improvement of the results from MW DM halo can be achieved by using longer exposure data (notably, longer exposure of the closed filter observations). In this paper, we improve our restrictions, coming from MW DM halo by using the blank sky dataset with better statistics from [25].

## II. DM WITH RADIATIVE DECAY CHANNEL

Although throughout this paper we are talking mostly about the sterile neutrino DM, the results can be applied to *any* DM particle, possessing the monoenergetic radiative decay channel, emitting photon of energy  $E_\gamma$  and having decay width  $\Gamma$ . In case of the sterile neutrino (with mass below that of electron), the radiative decay channel is into a photon and active neutrino [26]. As the mass of active neutrino is much smaller than keV, in this case  $E_\gamma = \frac{M_s}{2}$ . The width  $\Gamma$  of radiative decay can be expressed in terms of mass  $M_s$  and *mixing angle*  $\theta$  via [26, 27]:

$$\begin{aligned} \Gamma &= \frac{9\alpha G_F^2}{1024\pi^4} \sin^2 2\theta M_s^5 \\ &\simeq 1.38 \times 10^{-22} \sin^2(2\theta) \left[ \frac{M_s}{\text{keV}} \right]^5 \text{ sec}^{-1}. \end{aligned} \quad (1)$$

(although in all realistic cases  $\theta \ll 1$ , the notation  $\sin^2(2\theta)$  is used traditionally). The flux of the DM decay from a given direction is given by

$$F_{\text{DM}} = \Gamma \frac{E_\gamma}{M_s} \int_{\text{fov cone}} \frac{\rho_{\text{DM}}(\vec{r})}{4\pi |\vec{D}_L + \vec{r}|^2} d^3\vec{r}. \quad (2)$$

Here  $\vec{D}_L$  is the *luminous* distance between the observer and the center of the observed object,  $\rho_{\text{DM}}(r)$  is the DM density and the integration is over the DM distribution inside the (truncated) cone – solid angle, spanned by the field of view (FoV) of the X-ray satellite. If the observed object is far,<sup>1</sup> then Eq. (2) can be simplified:

$$F_{\text{DM}} = \frac{M_{\text{DM}}^{\text{fov}} \Gamma}{4\pi D_L^2} \frac{E_\gamma}{M_s}, \quad (3)$$

where  $M_{\text{DM}}^{\text{fov}}$  is the mass of DM within a telescope's field of view (FoV). Eq. (3) can be further rewritten as

$$\begin{aligned} F_{\text{DM}} &= 6.38 \times 10^6 \left( \frac{M_{\text{DM}}^{\text{fov}}}{10^{10} M_\odot} \right) \left( \frac{\text{kpc}}{D_L} \right)^2 \\ &\times \sin^2(2\theta) \left[ \frac{M_s}{\text{keV}} \right]^5 \frac{\text{keV}}{\text{cm}^2 \cdot \text{sec}}. \end{aligned} \quad (4)$$

In the absence of clearly detectable line, one can put upper limit on the flux of DM from the astrophysical data, which via Eq. (4) will lead to the restrictions of parameters of the sterile neutrino  $M_s$  and  $\theta$ .

## III. RESTRICTIONS FROM THE BLANK SKY OBSERVATION

### A. Modeling DM halo of the MW

As shown in the previous Section, to obtain the restrictions on parameters of the sterile neutrino, one needs to know the distribution of the DM. In case of nearby objects (including our own Galaxy and dwarf satellites from local halo), the DM distribution can be deduced e.g. by using the rotation curves of the stars in the galaxy. In particular, in Refs. [28, 29] it was shown that the DM halo of the MW can be described by Navarro-Frenk-White (NFW) profile [30]

$$\rho_{\text{NFW}}(r) = \frac{\rho_s r_s^3}{r(r + r_s)^2}, \quad (5)$$

with parameters, given in Table I.

One can also describe the DM distribution in the MW via isothermal profile:

$$\rho_{\text{iso}}(r) = \frac{v_h^2}{4\pi G_N} \frac{1}{r^2 + r_c^2} \quad (6)$$

The DM flux from a given direction  $\phi$  into the solid angle  $\Omega_{\text{fov}} \ll 1$ , measured by an observer on Earth (distance  $r_\odot \simeq 8$  kpc from the galactic center) is given by

$$F_{\text{DM}}^{\text{iso}}(\phi) = \frac{L_0}{R} \times \begin{cases} \frac{\pi}{2} + \arctan\left(\frac{r_\odot \cos \phi}{R}\right), & \cos \phi \geq 0 \\ \arctan\left(\frac{R}{r_\odot |\cos \phi|}\right), & \cos \phi < 0 \end{cases}. \quad (7)$$

Here  $L_0 \equiv \frac{\Gamma \Omega_{\text{fov}} v_h^2}{32\pi^2 G_N}$  and  $R = \sqrt{r_c^2 + r_\odot^2 \sin^2 \phi}$ . Angle  $\phi$  is related to the galactic coordinates  $(b, l)$  via

$$\cos \phi = \cos b \cos l. \quad (8)$$

Thus, galactic center corresponds to  $\phi = 0^\circ$ , anti-center  $\phi = 180^\circ$  and direction, perpendicular to the galactic plane to  $\phi = 90^\circ$ .

In Ref. [3] the following parameters of isothermal profile were chosen:  $v_h = 170$  km/sec and  $r_c = 4$  kpc. One can easily check (using Table I and Eqs. (A5)–(A6) in Appendix A) that in the directions  $\phi \gtrsim 90^\circ$  the difference in predicted DM fluxes between the NFW model with parameters, given in Table I and isothermal model with parameters just quoted are completely negligible (constitute less than 5%).<sup>2</sup>

<sup>1</sup> Namely, if luminosity distance  $D_L$  is much greater than the characteristic scale of the DM distribution  $\rho_{\text{DM}}(r)$ .

<sup>2</sup> Ref. [31] claimed that the MW results of Refs. [3, 4] are uncertain by about a factor of 3. This conclusion was based on the range of virial masses of the MW DM halo  $M_{\text{vir}} = (0.7 - 2.0) \times 10^{12} M_\odot$  in Ref. [28]. However, as just demonstrated, authors of [3] have chosen parameters of DM halo conservatively. The flux they used, corresponded to the favored models  $A_1$  or  $B_1$  in [28], with  $M_{\text{vir}} \sim 1.0 \times 10^{12} M_\odot$ . These models provide the *lowest* bound

References	$M_{\text{vir}}, M_{\odot}$	$r_{\text{vir}}, \text{kpc}$	Concentration	$r_s, \text{kpc}$	$\rho_s, M_{\odot}/\text{kpc}^3$
Klypin et al. [28], favored models ( $A_1$ or $B_1$ )	$1.0 \times 10^{12}$	258	12	21.5	$4.9 \times 10^6$
Battaglia et al. [29]	$0.8_{-0.2}^{+1.2} \times 10^{12}$	255	18	14.2	$11.2 \times 10^6$

TABLE I: Best fit parameters of NFW model of the MW DM halo (the relation between virial parameters and  $\rho_s$ ,  $r_s$  are given in Appendix A). Quoted halo parameters provide DM decay flux (from the directions with  $\phi > 90^\circ$ ) consistent within  $\sim 5\%$  with the one, given by Eqs. (6)–(7). Only “maximal disk” models in Klypin et al. [28] would provide 30–50% weaker restrictions, however, these models are highly implausible, see [28]. Similarly, taking lower limit for the virial mass of Battaglia et al. [29], one would obtain 25% weaker restrictions than the ones, presented in this paper.

## B. XMM-Newton PN blank sky data

We used the double-filtered single+double event XMM-Newton PN blank sky data from [25] – collection of 18 blank sky observations (see Table 2 in [25] for their observation IDs, positions and exposures).<sup>3</sup> The exposure time of the co-added observations is 547 ksec. We use a combination of closed filter observations from [25] (total exposure time 145 ksec) to model instrumental background of *XMM-Newton* PN instrument. The data has been filtered using SAS expression “flag==0” which rejects the data from bad pixels and CCD gap regions. After removing the brightest point sources the total accumulation area is 603 arcmin<sup>2</sup>.

The variable Galactic emission and geocoronal Solar wind charge exchange emission [32] complicate the modeling at the lowest energies. Also, due to the remaining calibration uncertainties (see e.g. [33]) we omitted the channels below 1.6 keV from our analysis. At energies above 7 keV the particle background dominates and the total flux is very sensitive to the background normalization. We thus excluded channels above 7 keV.

The data are not well described in the 2.3–2.6 and 5.9–6.3 keV bands if assuming only the power-law model for the CXRB. We can understand the former deviation by the fact that the PN total efficiency decreases by a factor of 2 at those energies and small calibration uncertainties can cause the effect. The latter deviation probably originates from the variability of the instrumental Fe line. Thus we excluded also these bands from further analysis.

We modeled the data in the remaining channels using a power-law model, modified at the lowest energies by Galactic absorption with the value of  $N_H$  fixed to its exposure weighted average over all blank sky observations ( $N_H = 1.3 \times 10^{20} \text{ cm}^{-2}$ ). The best-fit is acceptable, with reduced  $\chi^2 = 1.05$  for 25 degrees of freedom, yielding a

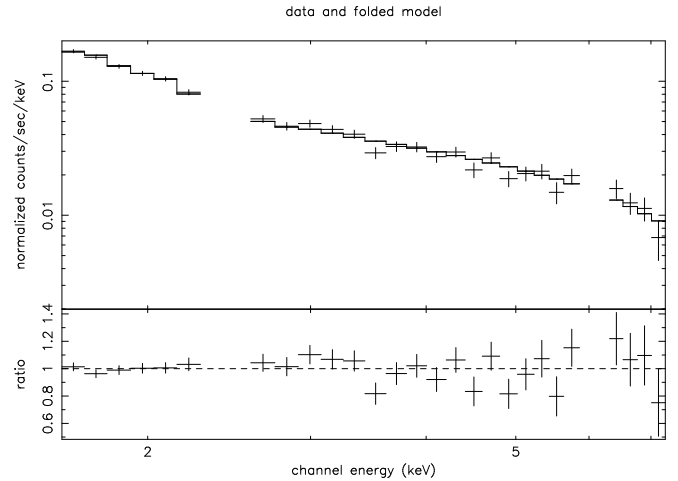


FIG. 1: Blank sky data of Nevalainen et al. [25], with closed filter data subtracted, together with the best-fit power law.

photon index of  $1.41 \pm 0.04$  at  $1\sigma$  confidence level (see FIG. 1), consistent with that obtained in similar analyses based on *Chandra* [34] and XMM-Newton MOS instrument [35].

The residuals do not exhibit any line-like features (see FIG. 1). To put bounds on the flux of DM, we rebin the data, so that each energy bin is equal to 2 times the spectral resolution of XMM and add the narrow Gaussian line at the center of every energy bin, until the fit worsens by  $\Delta\chi^2 = 9.0$  ( $3\sigma$  bound). The obtained flux per energy bin is then converted to the restrictions on  $M_s$  and  $\sin^2 2\theta$ , using Eqs. (1), (7) (we use exposure weighter average of DM fluxes (7) from all the observations, constituting the blank sky dataset). This corresponds to the average “column density”  $1.22 \times 10^{28} \text{ keV/cm}^2$ . The results are shown on FIG. 2. At energies above  $E = 5 \text{ keV}$  the instrumental background of PN dominates over the sky background (c.f. [25]). Therefore, the accuracy of the co-added closed filter spectrum in predicting the particle background in the blank sky observations becomes essential. We estimate this accuracy using the the variability of the individual closed filter spectra in the 1.6–7.0 keV band [25] and propagate it by varying the normalization of closed filter data by  $\pm 5\%$  and repeating the above analysis. This leads to a factor of 3 change of the results at  $M_s \sim 14 \text{ keV}$  (see FIG. 3). Therefore, for  $E \gtrsim 5 \text{ keV}$  we choose the more conservative normalization.

on derived flux of DM decay (if one does not take into account highly implausible “maximum disk” ( $A_2$  or  $B_2$ ) models of [28]). Even in the latter case, the DM flux will be 30–50% lower, than the one, used in work [3]. Therefore, parameters of MW DM halo from [3] provide the conservative estimate and we will use them in our work as well.

<sup>3</sup> We processed the blank sky data with newer SAS distribution, `xmmsoas_20050815_1803-6.5.0` and obtained slightly different exposure times than those in the public data.

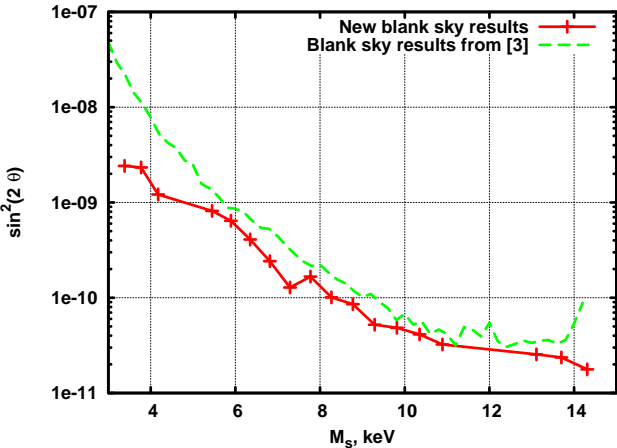


FIG. 2: Exclusion plot based on the blank sky observations.

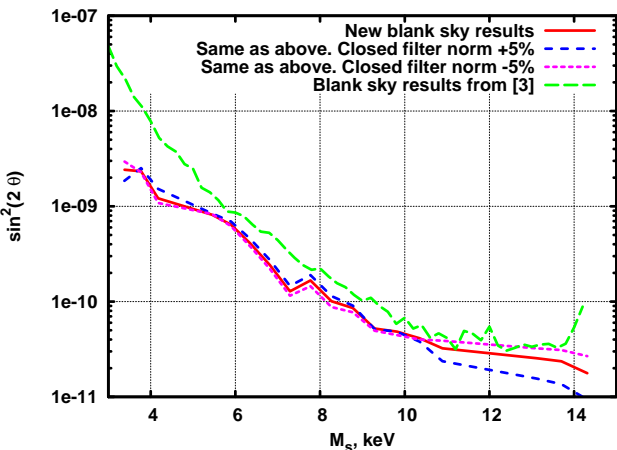


FIG. 3: Dependence of the results on closed filter normalization. Red (solid) and green (long-dashed) lines are the same as on the FIG. 2.

#### IV. RESTRICTIONS FROM OBSERVATIONS OF URSA MINOR

It was argued in Ref. [3] that dwarf satellite galaxies should provide the best restrictions, based on their high concentration of DM and low X-ray signal. At the moment of writing of [3] no public data on preferred dwarf satellites were available, therefore the observation of core of LMC were used as a demonstration. Recently, the Ursa Minor dwarf (UMi) was observed with *XMM-Newton* (obs IDs.: 0301690201, 0301690301, 0301690401, 0301690501, observed in August-September 2005).<sup>4</sup> Unfortunately, most of these observations are strongly contaminated by background flares and effectively have very

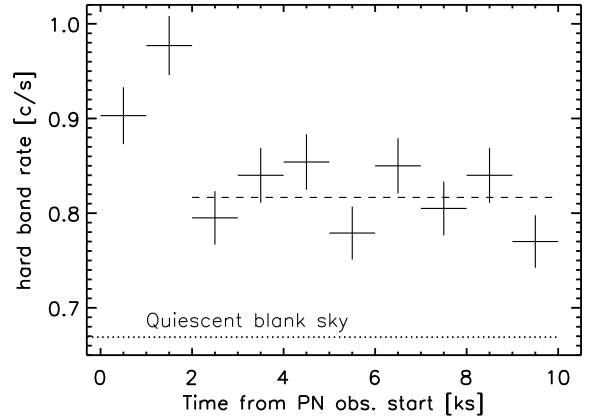


FIG. 4: The crosses show the PN >10 keV band rate of the full FOV during the Ursa Minor observation 0301690401 in 1ks bins. The dashed line shows the average, when excluding first 2 time bins. The dotted line shows the corresponding quiescent value in the co-added blank sky data Nevalainen et al. [25].

small exposure times. Below we present the analysis of only one observation (obsID: 0301690401), which “suffered” the least from background contamination.

##### A. DM modeling for UMi

The DM profile of UMi is well described by the isothermal profile (6) with parameters  $v_h = 22$  km/sec,  $r_c = 0.1$  kpc (see e.g. [36]). We adopt the distance to UMi  $D_L = 66$  kpc [37]. The DM mass within the circular FoV with the radius  $r_{\text{fov}}$ , centered at the center of the galaxy is given by

$$M_{\text{DM}}^{\text{fov}} = \frac{\pi v_h^2}{2G_N} \left( \sqrt{r_{\text{fov}}^2 + r_c^2} - r_c \right). \quad (9)$$

In our case, the radius of FoV is 13.9', which corresponds to  $r_{\text{fov}} = 0.27$  kpc (i.e. about  $3r_c$ ). Therefore

$$M_{\text{DM}}^{\text{fov}} = 3.3 \times 10^7 M_{\odot} \quad \text{for} \quad r_{\text{fov}} = 0.27 \text{ kpc}. \quad (10)$$

Using Eqs. (10) and (3) one can compute expected DM flux from UMi:

$$F_{\text{DM}} = 4.79 \frac{\text{keV}}{\text{cm}^2 \cdot \text{sec}} \left[ \frac{M_s}{\text{keV}} \right]^5 \sin^2(2\theta). \quad (11)$$

##### B. PN data analysis

We processed Ursa Minor observation 0301690401 using `epchain` version 8.56 and filtered the event file with SAS expressions “PATTERN<=4” and “FLAG==0”. We applied the blank sky based *XMM-Newton* background

<sup>4</sup> We are very grateful to Prof. T. Maccarone for sharing this data with us before it became publicly available through XMM data archive.

method of Nevalainen et al. [25] for Ursa Minor. The  $> 10$  keV band light curve from the full FOV (FIG. 4) shows that the count rate in observation 0301690401 (excluding first 2ks) exceeds that of the blank sky quiescent average by 25%. This level is higher, but close to that used in the blank sky accumulation ( $\pm 20\%$  filtering around the quiescent level). Thus we accepted the data from all instants after the initial 2ks, and we approximate the background uncertainties with those in Nevalainen et al. [25].

The hydrogen column density in the direction of Ursa Minor is small ( $\sim N_H = 2 \times 10^{20} \text{ cm}^{-2}$ ) and consistent with the variation in the blank sky sample. Thus we can apply the blank sky background method also to channels below 2 keV.

As noted in the above XMM-Newton blank sky study, the  $> 10$  keV band based scaling of the background only works up to a factor of 1.1, beyond which the background prediction becomes worse. Furthermore, the correlation of background rates in the  $> 10$  keV band is very poor with the rates below 2 keV band. Thus, in order to achieve best possible background prediction accuracy, we scaled the blank sky background spectrum by a factor of 1.1 at channels above 2 keV and at lower energies we applied no background scaling.

We removed such scaled background spectrum from the Ursa Minor spectrum (see FIG. 5). As shown in Nevalainen et al. [25], the background accuracy is worse at lower energies. We used those estimates to propagate the background uncertainties at  $1\sigma$  confidence level to our results by examining how the results change when varying the 0.8–2.0 keV and 2.0–7.0 keV band background by 15% and 10%, respectively.

### C. Ursa Minor data and restrictions on the sterile neutrino parameters

The X-ray spectrum of UMi is similar to that of LMC: above 2 keV the flux is zero within statistical limits (see FIG. 5). (Of course, the data set has rather low statistics – after the cleaning of flares the UMi observation contains only 7 ksec). Therefore, for such a data, we utilize the “total flux” method. Namely, we restrict the DM flux in the given energy bin to be bounded from above by the measured total flux in this energy bin plus its  $3\sigma$  uncertainty (solid black line on the FIG. 5). As every energy bin has width of twice the FWHM at a given energy, the flux from a DM line would not “spill” into nearby bins. Using Eq. (11), we find the restrictions on the sterile neutrino parameters, represented on FIG. 6 in red solid line.

These restrictions should be compared with those, obtained from another satellite galaxy – Large Magellanic Cloud – in Ref. [3]. As one clearly sees from FIG. 6, in spite of the low exposure time, it is fully consistent with the earlier bounds from LMC, thus confirming the results from [3]. Improvement of the exposure for UMi observations should, presumably lead to the improvement of

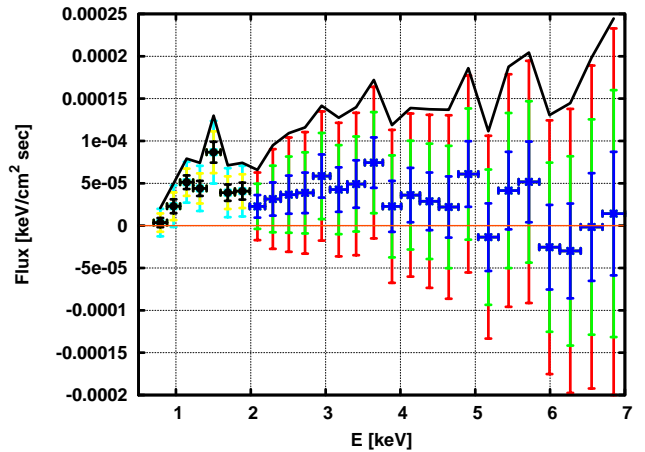


FIG. 5: Flux from UMi (obs. ID 0301690401). Energy bins have the width of twice the spectral resolution. Shown are 1, 2 and  $3\sigma$  errors. One can see that above 2 keV flux in the most energy bins is zero within  $1\sigma$  limits (blue crosses) and for the rest it is zero within  $2\sigma$  limits (green crosses). Similarly, below 2 keV black, cyan and yellow crosses represent 1,2 and  $3\sigma$  error correspondingly. Solid black line represents the  $3\sigma$  upper bound on total flux in a given energy bin, which we use to put the limit on DM parameters.

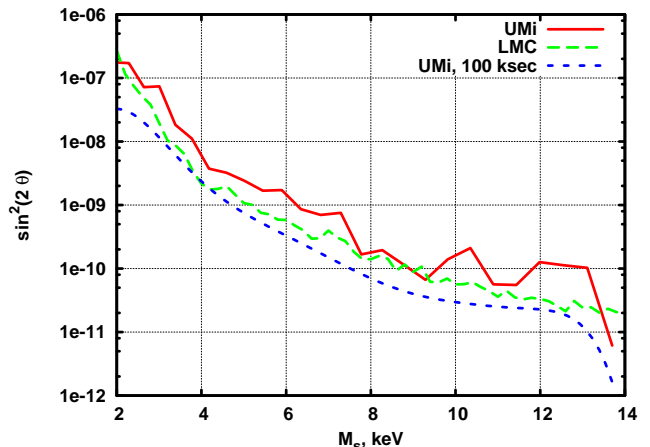


FIG. 6: Exclusion from UMi (red solid line), as compared to LMC (green long-dashed line). Blue short-dashed smooth curve shows hypothetical restrictions from UMi observations with 100 ksec exposure.

results (at least for energies above  $E \gtrsim 2$  keV). For example, for a 100 ksec observation, we expect the results to improve by roughly a factor  $\sqrt{100 \text{ ksec}/7 \text{ ksec}} \approx 3.77$ .

## V. RESULTS

### 1. Restrictions from the blank sky data

By analyzing the blank sky data set with better statistics, we improved the previous results [3, 4, 5] (by as

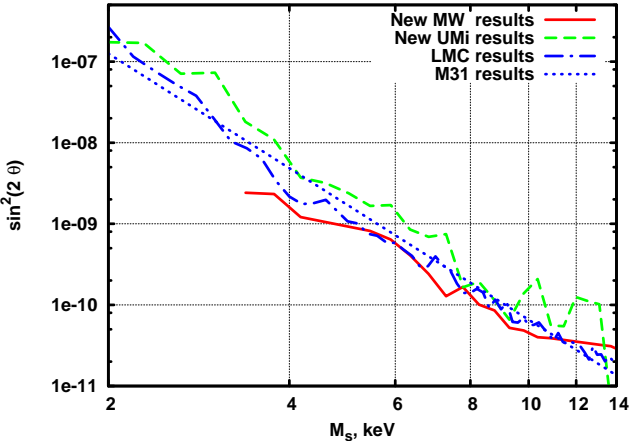


FIG. 7: Results and comparison with previous bounds (a region of parameter space *above* a curve is excluded)

much as the factor of 10 for  $M_s \approx 3.5$  keV and by the negligible amount for  $M_s \gtrsim 11$  keV). The result is shown on FIG. 7 in red solid line. Best previous bounds are also shown: bound from LMC [3] in blue short-dashed line and bound from M31 [5] in dotted magenta line. We see that in the region  $3.5 \text{ keV} \lesssim M_s \lesssim 11 \text{ keV}$  new blank sky data provides an improvement over previous results. These results can be converted (using Eq. (1)) into restrictions on the decay rate  $\Gamma$  of *any* DM particle, possessing radiative decay channel and emitting a photon  $E_\gamma$  (see FIG. 8). Our results provide more than an order of magnitude improvement over similar restrictions derived in [4] (which used the *Chandra* blank sky background), as one can clearly see by comparing FIG. 8 with the FIG. 2 in [4], where exclusion plot is above  $\Gamma = 10^{-26} \text{ sec}^{-1}$  line for all energies. (In Ref. [4] the restriction were made, based on the total flux of *Chandra* satellite, without subtraction of the instrumental background, which explains a much weaker restrictions).

The empirical fit to the MW data is given by the following expression:

$$\sin^2(2\theta) \lesssim 2.15 \times 10^{-7} \left( \frac{M_s}{\text{keV}} \right)^{-3.45}. \quad (12)$$

## 2. Restrictions from Ursa Minor dwarf

Restrictions from XMM observation of UMi are shown on FIG. 7 in the green long-dashed line. These results are slightly weaker, than LMC or M31 results, which is due to the very low statistics of the UMi observation. Improvement of the statistics should lead to improvement of the current bound (as shown on the FIG. 6). These results confirm the recent claims [3] that dwarfs of the Local Halo are promising candidates for the DM decay line search and as such should be studied dedicatedly.

In searching for the DM signatures, it is important to understand that the uncertainties of the DM modeling

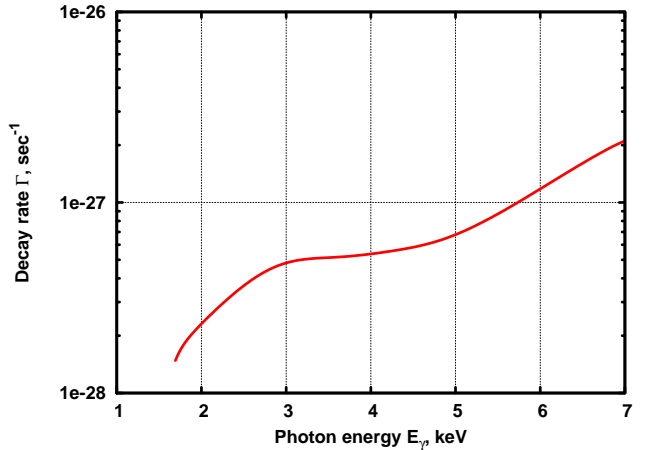


FIG. 8: Restrictions on parameters of any DM particle with the radiative decay width  $\Gamma$ , emitting photon of energy  $E_\gamma$ . Region above the red curve is excluded.

for any given object can be large and therefore it is important to study many objects of given type as well as many different types of objects (where DM distributions are deduced by independent methods). To this end, although UMi data does not provide an improvement over existing bounds, it makes those bounds more robust as the existence of DM in UMi is deduced by independent observations and the rotation curves of UMi are measured quite well, since it has less perturbed dynamics, compared to e.g. LMC.

## VI. DISCUSSION

In this paper we continued to search for the best astrophysical objects, from the point of view of restricting parameters of DM particles with radiative decay channel. Several comments are of order here.

- (1) Although throughout this paper we spoke about the sterile neutrinos and restricted their parameters (namely, mass and mixing angle), the constraints can be readily converted into any other DM candidate, which possesses a radiative decay channel. Then the restrictions are formulated on the decay rate  $\Gamma$  as a function of energy of emitted photon  $E_\gamma$ . The results then can be presented in the form of exclusion plot, presented on FIG. 8.
- (2) Clearly, if one could relate parameters of the sterile neutrino with their relic abundance  $\Omega_s$ , this would allow one to put an upper limit on the mass of the sterile neutrino. Unfortunately, such a computation is strongly model-dependent. In [7, 8, 38, 39] the relic abundance of the sterile neutrinos was computed in a simple model with only one sterile neutrino. Yet, even the computation in this simplest model is subject to a number of uncertainties [1, 3, 40, 41, 42, 43]. In particular, in [7, 8, 38, 39] it was assumed (*i*) the

absence of the sterile neutrinos above the temperatures  $\sim 1$  GeV; (ii) the absence of heavy particles, whose decay can dilute the relic abundance; (iii) the absence of leptonic asymmetries. In addition, simplifying assumptions about dynamics of hadrons at temperatures  $\mathcal{O}(150)$  MeV were used. Taking away these assumptions makes the relation between  $\Omega_s$ ,  $M_s$  and  $\theta$  uncertain by several orders of magnitude [40, 41, 42, 43]. Therefore, in this work we chose not to put an upper bound on the mass of the sterile neutrino.

### Acknowledgements

We would like to thank A. Neronov, M. Markevitch, I. Tkachev, M. Shaposhnikov for help during the various stages of this project. J.N. acknowledges the support from the Academy of Finland. The work of O.R. was supported in part by European Research Training Network contract 005104 “ForcesUniverse” and by a *Marie Curie International Fellowship* within the 6<sup>th</sup> European Community Framework Programme.

### APPENDIX A: DETERMINING PARAMETERS OF NFW PROFILE

Using the data on rotation curves, one usually obtains the following parameters of DM distribution (see e.g. [28]): virial mass  $M_{\text{vir}}$ , virial radius  $r_{\text{vir}}$  and concentration parameter  $C$ . They have the following relation with the parameters of NFW profile (5)  $r_s$  and  $\rho_s$ :

$$r_s = \frac{r_{\text{vir}}}{C}; \quad \rho_s = \frac{M_{\text{vir}}}{4\pi r_s^3 f(C)}, \quad (\text{A1})$$

where in terms of function  $f(x)$ :

$$f(x) = \log(1 + x) - \frac{x}{1 + x} \quad (\text{A2})$$

one obtains the mass within the radius  $r$ :

$$M(r) = M_{\text{vir}} \frac{f(r/r_s)}{f(C)}. \quad (\text{A3})$$

If DM distribution in the Milky Way is described by NFW model (as in [28, 29], the flux from a direction  $\phi$  is given by

$$F_{\text{DM}}^{\text{NFW}}(\phi) = \frac{\Gamma\Omega_{\text{fov}}}{8\pi} \int_0^\infty dz \rho_{\text{NFW}}(\sqrt{r_\odot^2 + z^2 + 2r_\odot z \cos\phi}) \quad (\text{A4})$$

(notations are the same as in Eq.(7)–(8)). Let us consider two cases, when the integral in (A4) can be easily computed. Namely, we have for  $\phi = 180^\circ$

$$F_{\text{DM}}^{\text{NFW}}(180^\circ) = \frac{\Gamma\Omega_{\text{fov}}}{8\pi} \rho_s r_s \left[ \log\left(1 + \frac{r_s}{r_\odot}\right) - \frac{r_s}{r_s + r_\odot} \right] \quad (\text{A5})$$

and for  $\phi = 90^\circ$

$$F_{\text{DM}}^{\text{NFW}}(90^\circ) = \frac{\Gamma\Omega_{\text{fov}}}{8\pi} \rho_s r_s \left[ -1 - \log\frac{2r_s}{r_\odot} + \frac{r_\odot^2}{r_s^2} \left( \frac{3}{2} \log\frac{2r_s}{r_\odot} - \frac{5}{4} \right) \right] + \mathcal{O}\left(\frac{r_\odot^4}{r_s^4}\right) \quad (\text{A6})$$

(in the latter case the analytic expression is too complicated and we present Taylor expansion for the case  $r_\odot \ll r_s$ ).

---

[1] A. Boyarsky, A. Neronov, O. Ruchayskiy, and M. Shaposhnikov, MNRAS **370**, 213 (2006), astro-ph/0512509.  
[2] A. Boyarsky, A. Neronov, O. Ruchayskiy, and M. Shaposhnikov (2006), astro-ph/0603368.  
[3] A. Boyarsky, A. Neronov, O. Ruchayskiy, M. Shaposhnikov, and I. Tkachev (2006), astro-ph/0603660.  
[4] S. Riemer-Sørensen, S. H. Hansen, and K. Pedersen, ApJ **644**, L33 (2006), astro-ph/0603661.  
[5] C. R. Watson, J. F. Beacom, H. Yuksel, and T. P. Walker, Phys. Rev. **D74**, 033009 (2006), astro-ph/0605424.  
[6] S. Riemer-Sørensen, K. Pedersen, S. H. Hansen, and H. Dahle (2006), astro-ph/0610034.  
[7] S. Dodelson and L. M. Widrow, Phys. Rev. Lett. **72**, 17 (1994), hep-ph/9303287.  
[8] A. D. Dolgov and S. H. Hansen, Astropart. Phys. **16**, 339 (2002), hep-ph/0009083.  
[9] K. Abazajian, G. M. Fuller, and W. H. Tucker, Astrophys. J. **562**, 593 (2001), astro-ph/0106002.  
[10] A. Strumia and F. Vissani (2006), hep-ph/0606054.  
[11] T. Asaka, S. Blanchet, and M. Shaposhnikov, Phys. Lett. **B631**, 151 (2005), hep-ph/0503065.  
[12] T. Asaka and M. Shaposhnikov, Phys. Lett. **B620**, 17 (2005), hep-ph/0505013.  
[13] P. Bode, J. P. Ostriker, and N. Turok, Astrophys. J. **556**, 93 (2001), astro-ph/0010389.  
[14] T. Goerdt, B. Moore, J. I. Read, J. Stadel, and M. Zemp, MNRAS **368**, 1073 (2006), astro-ph/0601404.  
[15] U. Seljak, A. Makarov, P. McDonald, and H. Trac (2006), astro-ph/0602430.  
[16] M. Viel, J. Lesgourgues, M. G. Haehnelt, S. Matarrese, and A. Riotto, Phys. Rev. Lett. **97**, 071301 (2006), astro-ph/0605707.  
[17] L. E. Strigari et al. (2006), astro-ph/0603775.  
[18] S. H. Hansen, J. Lesgourgues, S. Pastor, and J. Silk, MNRAS **333**, 544 (2002), astro-ph/0106108.  
[19] M. Viel, J. Lesgourgues, M. G. Haehnelt, S. Matarrese, and A. Riotto, Phys. Rev. **D71**, 063534 (2005), astro-ph/0501562.  
[20] A. Kusenko (2006), hep-ph/0609081.  
[21] P. L. Biermann and A. Kusenko, Phys. Rev. Lett. **96**, 091301 (2006), astro-ph/0601004.  
[22] J. Stasielak, P. L. Biermann, and A. Kusenko (2006),

astro-ph/0606435.

[23] A. Kusenko (2006), astro-ph/0609375.

[24] J. Hidaka and G. M. Fuller (2006), astro-ph/0609425.

[25] J. Nevalainen, M. Markevitch, and D. Lumb, *Astrophys. J.* **629**, 172 (2005), astro-ph/0504362.

[26] P. B. Pal and L. Wolfenstein, *Phys. Rev. D* **25**, 766 (1982).

[27] V. D. Barger, R. J. N. Phillips, and S. Sarkar, *Phys. Lett. B* **352**, 365 (1995), hep-ph/9503295.

[28] A. Klypin, H. Zhao, and R. S. Somerville, *ApJ* **573**, 597 (2002), astro-ph/0110390.

[29] G. Battaglia et al., *Mon. Not. Roy. Astron. Soc.* **364**, 433 (2005), astro-ph/0506102.

[30] J. F. Navarro, C. S. Frenk, and S. D. M. White, *Astrophys. J.* **490**, 493 (1997), astro-ph/9611107.

[31] K. Abazajian and S. M. Koushiappas, *Phys. Rev. D* **74**, 023527 (2006), astro-ph/0605271.

[32] B. J. Wargelin, M. Markevitch, M. Juda, V. Kharchenko, R. Edgar, and A. Dalgarno, *ApJ* **607**, 596 (2004), astro-ph/0402247.

[33] J. Nevalainen, M. Bonamente, and J. Kaastra, ArXiv Astrophysics e-prints (2006), astro-ph/0610461.

[34] R. C. Hickox and M. Markevitch, *ApJ* **645**, 95 (2006), astro-ph/0512542.

[35] A. De Luca and S. Molendi, *Astron. Astrophys.* **419**, 837 (2004), astro-ph/0311538.

[36] M. I. Wilkinson et al. (2006), astro-ph/0602186.

[37] M. L. Mateo, *ARA&A* **36**, 435 (1998), astro-ph/9810070.

[38] K. Abazajian, G. M. Fuller, and M. Patel, *Phys. Rev. D* **64**, 023501 (2001), astro-ph/0101524.

[39] K. Abazajian, *Phys. Rev. D* **73**, 063506 (2006), astro-ph/0511630.

[40] X.-d. Shi and G. M. Fuller, *Phys. Rev. Lett.* **82**, 2832 (1999), astro-ph/9810076.

[41] T. Asaka, A. Kusenko, and M. Shaposhnikov, *Phys. Lett. B* **638**, 401 (2006), hep-ph/0602150.

[42] T. Asaka, M. Laine, and M. Shaposhnikov, *JHEP* **06**, 053 (2006), hep-ph/0605209.

[43] M. Shaposhnikov and I. Tkachev, *Phys. Lett. B* **639**, 414 (2006), hep-ph/0604236.